

Simulation of structural and electronic properties of amorphous tungsten oxycarbides

Kaliappan Muthukumar, Roser Valentí, Harald O. Jeschke

Institut für Theoretische Physik, Goethe-Universität Frankfurt am Main, 60438
Frankfurt am Main, Germany

E-mail: jeschke@itp.uni-frankfurt.de

Abstract. Electron beam induced deposition with tungsten hexacarbonyl $W(CO)_6$ as precursors leads to granular deposits with varying compositions of tungsten, carbon and oxygen. Depending on the deposition conditions, the deposits are insulating or metallic. We employ an evolutionary algorithm to predict the crystal structures starting from a series of chemical compositions that were determined experimentally. We show that this method leads to better structures than structural relaxation based on guessed initial structures. We approximate the expected amorphous structures by reasonably large unit cells that can accommodate local structural environments that resemble the true amorphous structure. Our predicted structures show an insulator to metal transition close to the experimental composition at which this transition is actually observed. Our predicted structures also allow comparison to experimental electron diffraction patterns.

PACS numbers: 71.15.Mb, 61.46.-w, 61.43.Dq

1. Introduction

Nanotechnological applications require fabrication of nanometer-sized structures on various substrates. Electron beam induced deposition (EBID) has emerged as a promising technique to make nanostructures in a size, shape and position-controlled manner without the use of any expensive masks [1, 2, 3, 4, 5]. Deposits with the desired metal content and electronic properties can be obtained either directly by tuning the preparation conditions (varying electron beam energy or current or raster current) or by post-fabrication techniques (heating or further irradiation). Thus fabrication of materials with new physical and chemical properties at the nanoscale has been successfully achieved [3, 5, 6, 7, 8, 9, 10].

Transition metal carbides possess unique physical and chemical properties that have made them promising materials in several industrial and electronic applications. The composition of tungsten granular deposits obtained by decomposing $W(CO)_6$ as a precursor in the EBID process indicates that the tungsten atoms are embedded in a carbon (and oxygen) matrix [3]. Although investigations on the microstructure and the electrical transport properties have shed some light on the behavior of these systems, a deep microscopic understanding is still missing.

Several theoretical studies are available on the structural and electronic properties of $4d$ and $5d$ transition metal carbides [11, 12]. Nevertheless, studies on metal oxycarbides are scarce due to the lack of knowledge on their structures. The high level of carbon and oxygen concentrations up to an average of 30-40% in the EBID-fabricated samples indicates that a good description of the electronic structure of these metal oxycarbides may be obtained by suitably guessing approximate structures from the well-known crystal structures of tungsten carbides and tungsten oxides. This methodology indeed has been successful in predicting the structure of Pt_2Si_3 derived from Pt_2Sn_3 [13]. A similar procedure for tungsten oxycarbides has been adapted by Suetin *et al.*, who investigated the structure, electronic and magnetic properties of some tungsten oxycarbides by constructing approximate crystal structures obtained from systematically replacing the carbon by oxygen in the hexagonal structure of WC and oxygen by carbon in the cubic structure WO_3 [14]. However, a powerful evolutionary algorithm was recently proposed which in principle can predict the crystal structure of materials with any atomic composition and is not biased by the choice of initially known crystal structure settings [15, 16, 17].

In the present work we use this evolutionary algorithm to predict structures of approximants to amorphous tungsten oxycarbides as obtained by the EBID process. By analyzing the electronic properties of our predicted structures, we find an insulator to metal transition at a composition close to the composition where experimentally such a transition has been observed [6]. We further show that the calculated X-ray diffraction patterns (XRD) for our structures correlate very well with the patterns measured experimentally [3, 6].

2. Method

We approximated the amorphous tungsten oxycarbides structures obtained in the EBID process by large unit cells that can account for the local structural environment present in the experimental compositions. In order to predict these structures, we employed evolutionary algorithms developed by A. Oganov *et al.* featuring local optimization, real-space representation and flexible physically motivated variation operators [15, 16, 17]. Each generation contained between 20 and 40 structures and the first generation was always produced randomly. Three different sets of calculation have been performed for each composition with differing number of initial populations and varying slightly the parameter (fracPerm) that controls the percentage of structures obtained by heredity and permutation. With all these different sets of calculation, ca. 2000 structures were screened for each composition. All structures were locally optimized during structure search using density functional theory (DFT) with the projector augmented wave (PAW) [18, 19] as implemented in VASP [19, 20, 21, 22]. The generalized gradient approximation (GGA) in the parametrization of Perdew, Burke and Ernzerhof [23] was used as approximation for the exchange and correlation functional. The reported structures are the ones with the lowest enthalpy; the evolutionary algorithm was considered converged when the lowest enthalpy structure couldn't be improved during eight generations. We analyzed the electronic structure of the resulting structures using the full potential local orbital (FPLO) basis [24]. The XRD patterns were simulated by the Reflex module implemented in Materials Studio package.

3. Results and Discussion

Sample	W	C	O	approximant	approximant composition
1	19.0	67.1	13.8	$W_3C_{10}O_2$	$WC_{3.33}O_{0.67}$
2	22.6	56.0	21.4	$W_2C_5O_2$	$WC_{2.5}O$
3	27.5	50.4	22.1	$W_4C_7O_3$	$WC_{1.75}O_{0.75}$
4	31.8	44.4	23.8	$W_5C_7O_4$	$WC_{1.4}O_{0.8}$
5	34.0	44.3	21.7	$W_3C_4O_2$	$WC_{1.33}O_{0.67}$
6	36.9	35.6	27.5	$W_7C_7O_5$	$WCO_{0.71}$

Table 1. EBID obtained samples as reported in Ref. [6] and the corresponding approximant used for the structure prediction are listed. The concentrations are given in atomic %. The composition of the approximants normalized to the tungsten content is also listed.

We first tested the method of evolutionary algorithm-based structure prediction using some known tungsten structures. As an example, we verified that USPEX indeed predicts the known hexagonal structure of WC [26]. Next, we address the problem of predicting crystalline tungsten oxycarbides. This has recently been discussed by Suetin

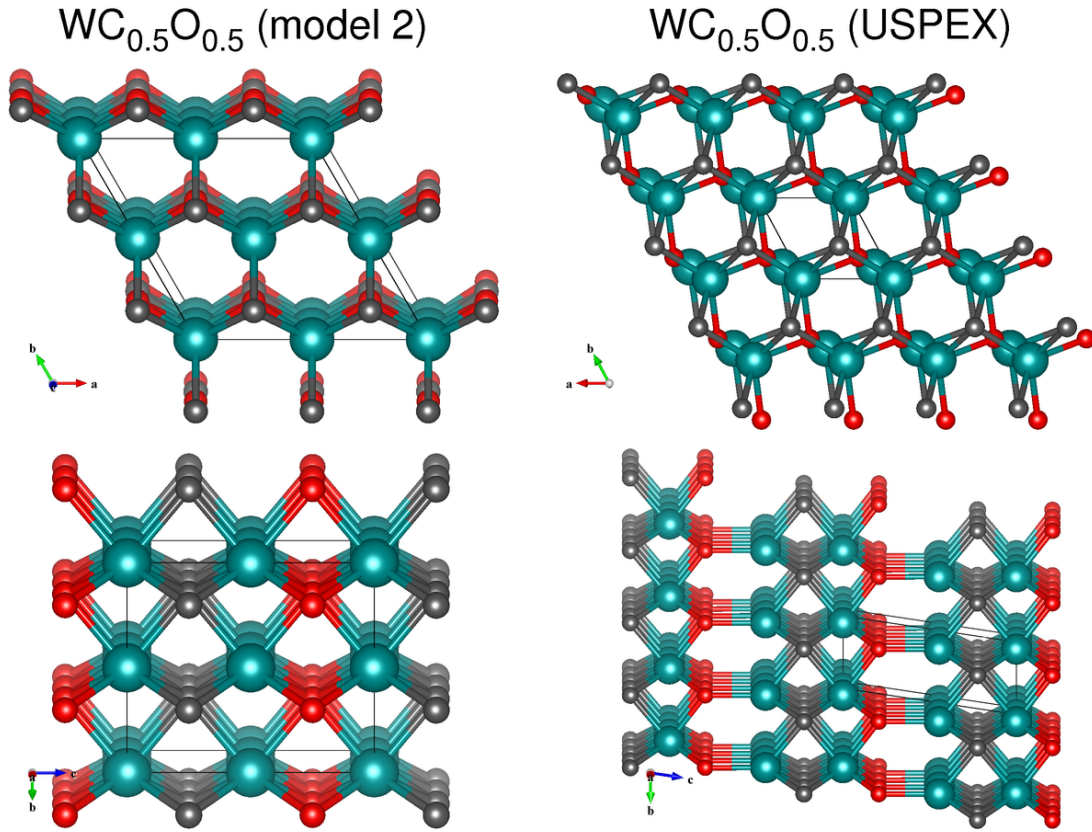


Figure 1. Predicted structures for the tungsten oxycarbide $\text{WC}_{0.5}\text{O}_{0.5}$. Left: Best structure obtained by relaxing guessed candidate structures. Right: USPEX result.

et al. [14] for the examples $\text{WC}_{1-x}\text{O}_x$ and $\text{WC}_{3-x}\text{O}_x$. The authors successively replace carbon atoms in WC with oxygen and replace oxygen atoms in WO_3 by carbon atoms and relax the resulting structure candidates using the full potential linearized augmented plane wave (FPLAPW) basis set. We verified that the structure of $\text{WC}_{0.5}\text{O}_{0.5}$ with alternating layers of WC and WO (Fig. 1 (left)) indeed is the optimal structure also when relaxing different structure candidates using VASP. We then performed an USPEX structure prediction with the composition W_2CO . This yields as optimum the structure shown in Fig. 1 (right). It is triclinic ($P1$ symmetry) and it is 1.35 eV per W_2CO unit lower in energy than the high symmetry ($P-6m2$) structure obtained by relaxing structure candidates (Fig. 1 (left)). This indicates that indeed it is preferable to avoid bias by using a structure search based on evolutionary principles.

Figs. 2 and 3 show the optimal structures we obtained. The samples with high carbon content show inclusions of regions that resemble diamond-like carbon (sample 1) or graphitic carbon (samples 2 and 4). This leads to a lower density as can be seen from Fig. 4 in which the density of amorphous tungsten oxycarbide approximants is plotted against the metal content. On the one hand, there is a weak overall proportionality of density with tungsten content, illustrated by the line fitted to the six data points. On the other hand, samples 1, 2 and 4 fall into a lower density group ($\text{WC}_{3.33}\text{O}_{0.67}$, $\text{WC}_{2.5}\text{O}$ and $\text{WC}_{1.4}\text{O}_{0.8}$, ρ from 7.8 g/cm^3 to 9.1 g/cm^3) which shows some phase separation between

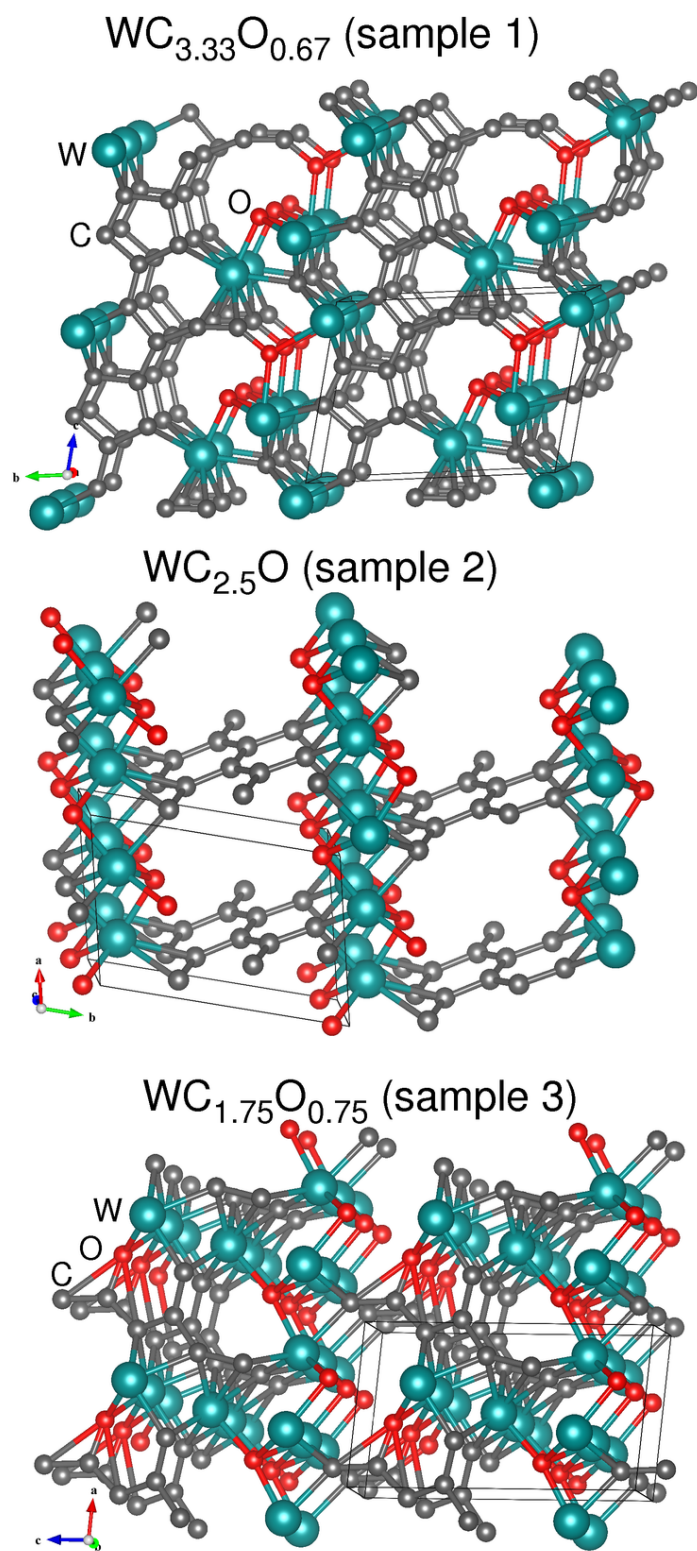


Figure 2. Predicted tungsten oxycarbide structures for the compositions $WC_{3.33}O_{0.67}$, $WC_{2.5}O$ and $WC_{1.75}O_{0.75}$.

low carbon content tungsten oxycarbide and regions of pure carbon, and a higher density

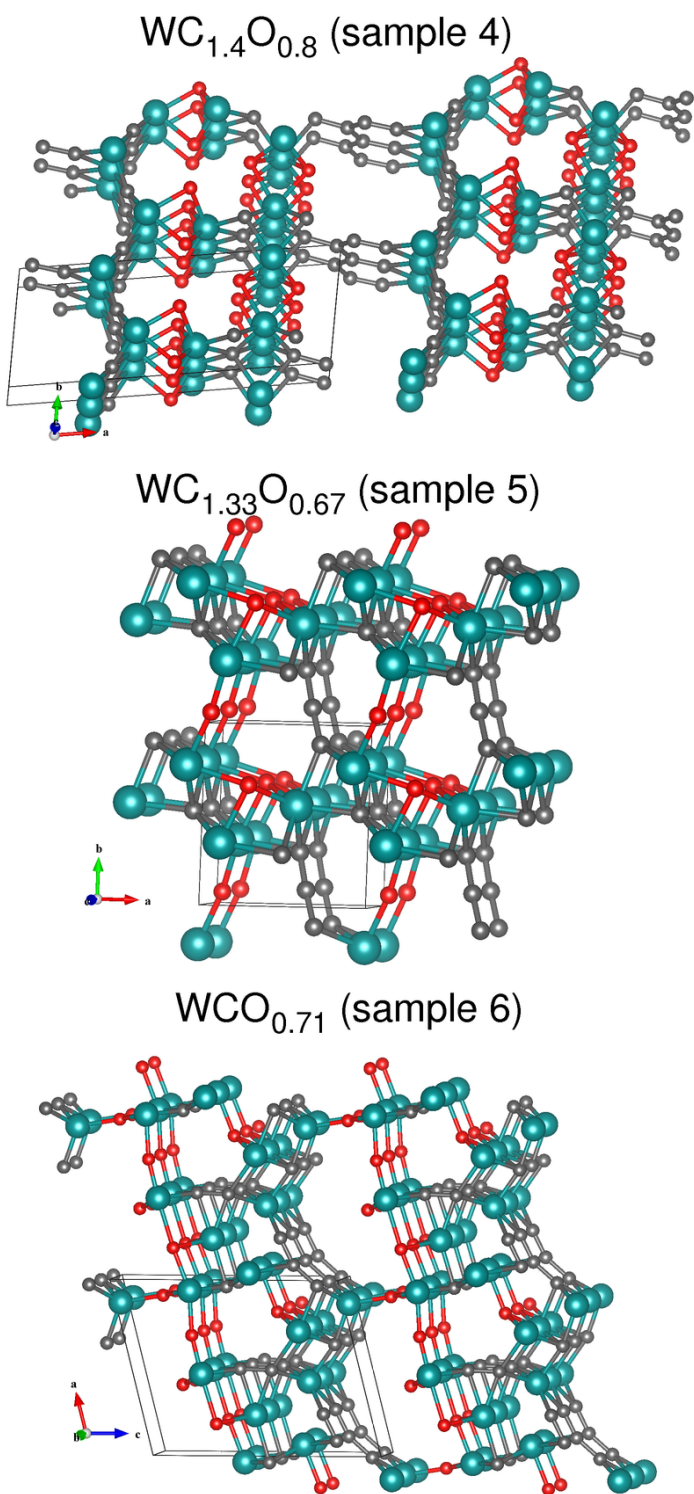


Figure 3. Predicted tungsten oxycarbide structures for the compositions WC_{1.4}O_{0.8}, WC_{1.33}O_{0.67} and WCO_{0.71}.

group, samples 3, 5 and 6 (WC_{1.75}O_{0.75}, WC_{1.33}O_{0.67} and WCO_{0.71}, ρ from 10.0 g/cm³ to 10.7 g/cm³) which is more homogeneous and more highly coordinated.

We now investigate the electronic structure of the predicted amorphous tungsten

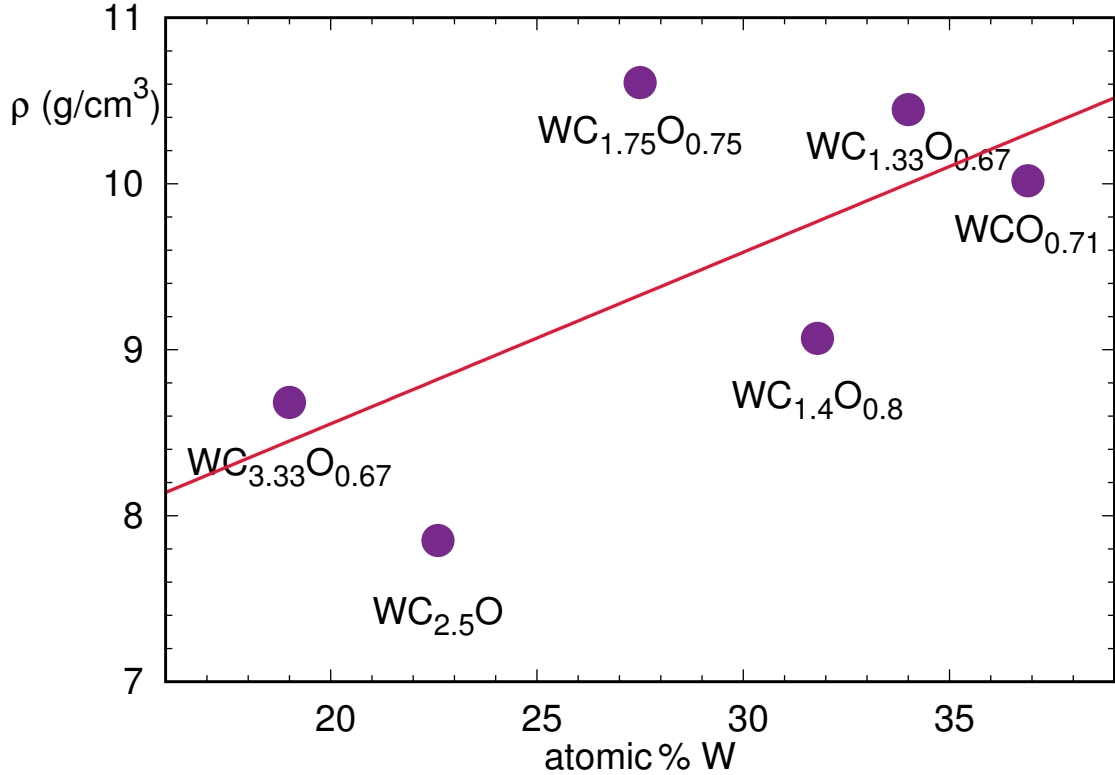


Figure 4. The density of the predicted tungsten oxycarbide structures roughly increases with tungsten content.

oxycarbide approximants. We employ the FPLO basis [24] within GGA. Due to the large mass of tungsten, we compared scalar relativistic and fully relativistic electronic structure calculations. We find significant splittings due to spin-orbit coupling in all bandstructures, and therefore in the following we base our analysis on fully relativistic calculations. Fig. 5 shows a comparison of the densities of states of the six materials with tungsten, carbon and oxygen contributions shown in different colors. We immediately observe an insulator-to-metal transition between sample 2 (WC_{2.5}O) and sample 3 (WC_{1.75}O_{0.75}) which corresponds to a transition between 22% and 29% metal content. This is in excellent agreement with the observation of Ref. [6] where the conductivity measurements on the six samples (see Table 1) showed a change from insulating to metallic behaviour between sample 3 and sample 4. In fact, Fig. 2 of Ref. [6] shows that sample 3 takes an intermediate position between clearly finite conductivity in the $T \rightarrow 0$ limit for sample 4 and clearly vanishing conductivity in the $T \rightarrow 0$ limit for sample 2.

For comparison we present in Fig. 6 the densities of states for the predicted crystalline structure of our test system W₂CO as well as for the known structures of WO₂ (Ref. [25]) and WC (Ref. [26]). We observe a qualitatively different behavior for the three structures.

In Figs. 7 and 8, we show the calculated bandstructures for the first four predicted structures. Here, we can also clearly see the transition from insulating to metallic behaviour upon increase of tungsten content as well as the splitting of the bands due to

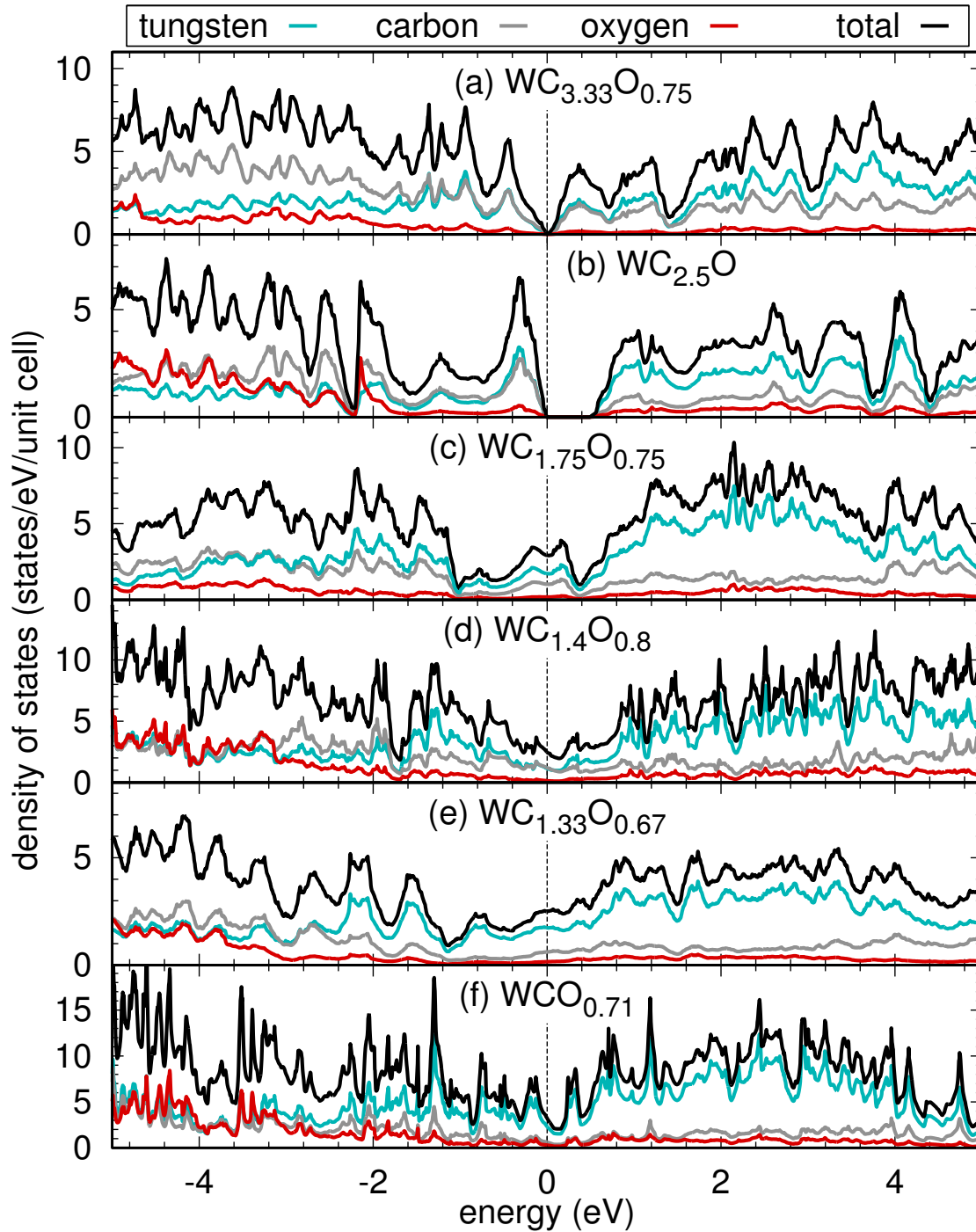


Figure 5. Electronic density of states of the predicted tungsten oxycarbide structures.

the spin-orbit coupling. We also observe highly dispersive bands which is a signature of the three-dimensionality of the systems.

In order to check how good our simulated structures describe the amorphous deposits, we present in Figs. 9 and 10 the pair correlation functions of the first four predicted structures. The contributions of bonds involving tungsten are highlighted. The pair correlation function first shows carbon-carbon bonds at 1.4-1.5 Å indicating

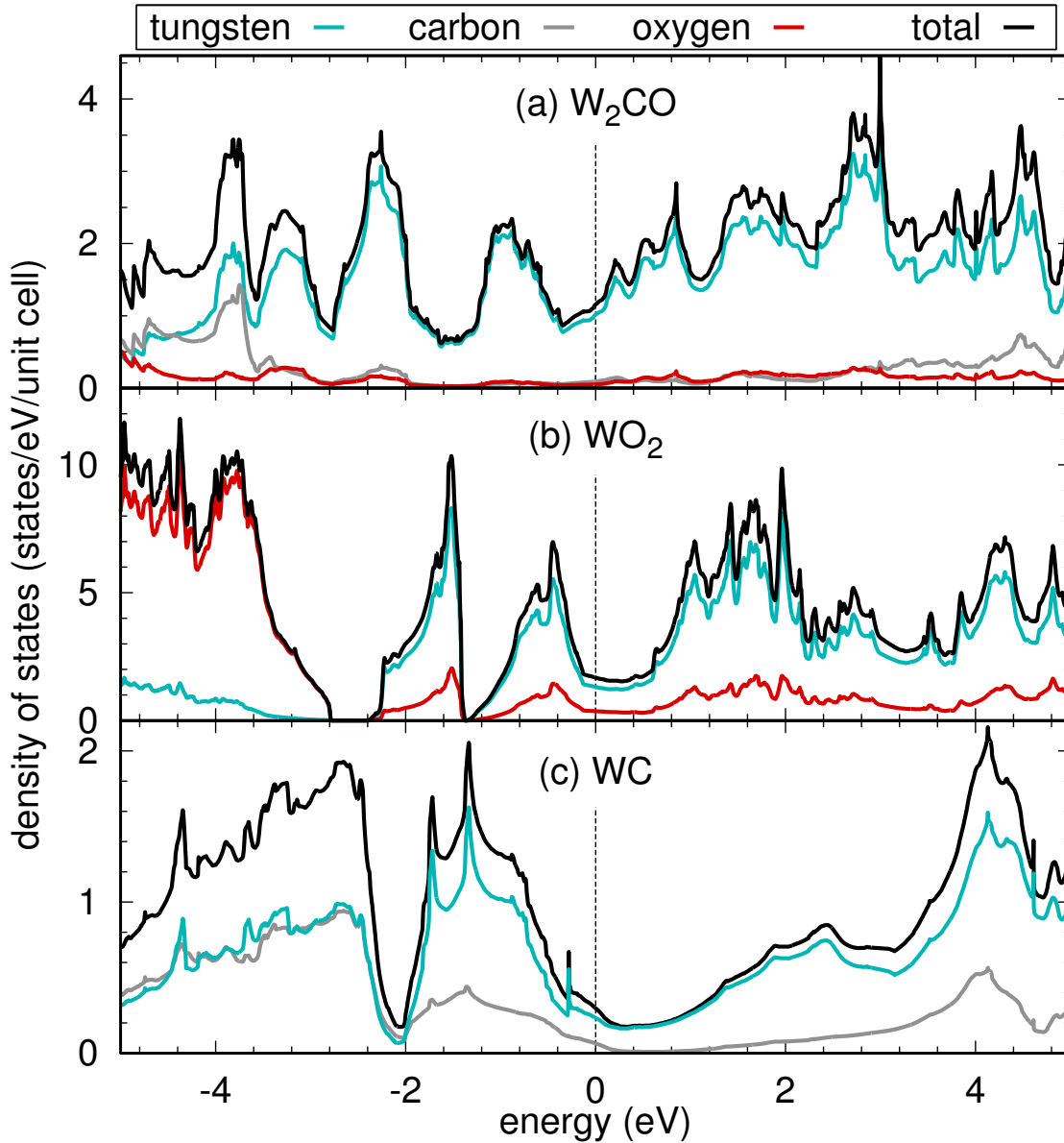


Figure 6. Electronic density of states of (a) the predicted structure of W_2CO and of the known crystalline structures of (b) WO_2 and (c) WC .

that the matrix is composed of carbon atoms with sp^2 and sp^3 hybridization which is in accordance with the experimental evidence based on micro-Raman measurements on tungsten-based composites obtained in the EBID process [27]. Further analysis indicates that at 2.0 Å, there are W-O bonds, followed by W-C bonds at slightly larger distances. The first W-W bonds are seen at 2.6 Å.

Finally, we can compare our predicted structures to experiment by calculating the electron diffraction patterns. Fig. 11 shows the predicted electron diffraction patterns for electrons with an energy of 300 keV. The experimental data shown in the figure are from Ref. [27]. We find a very good agreement between the main peak observed experimentally at 4 nm^{-1} and the peaks in the predicted diffraction patterns. This

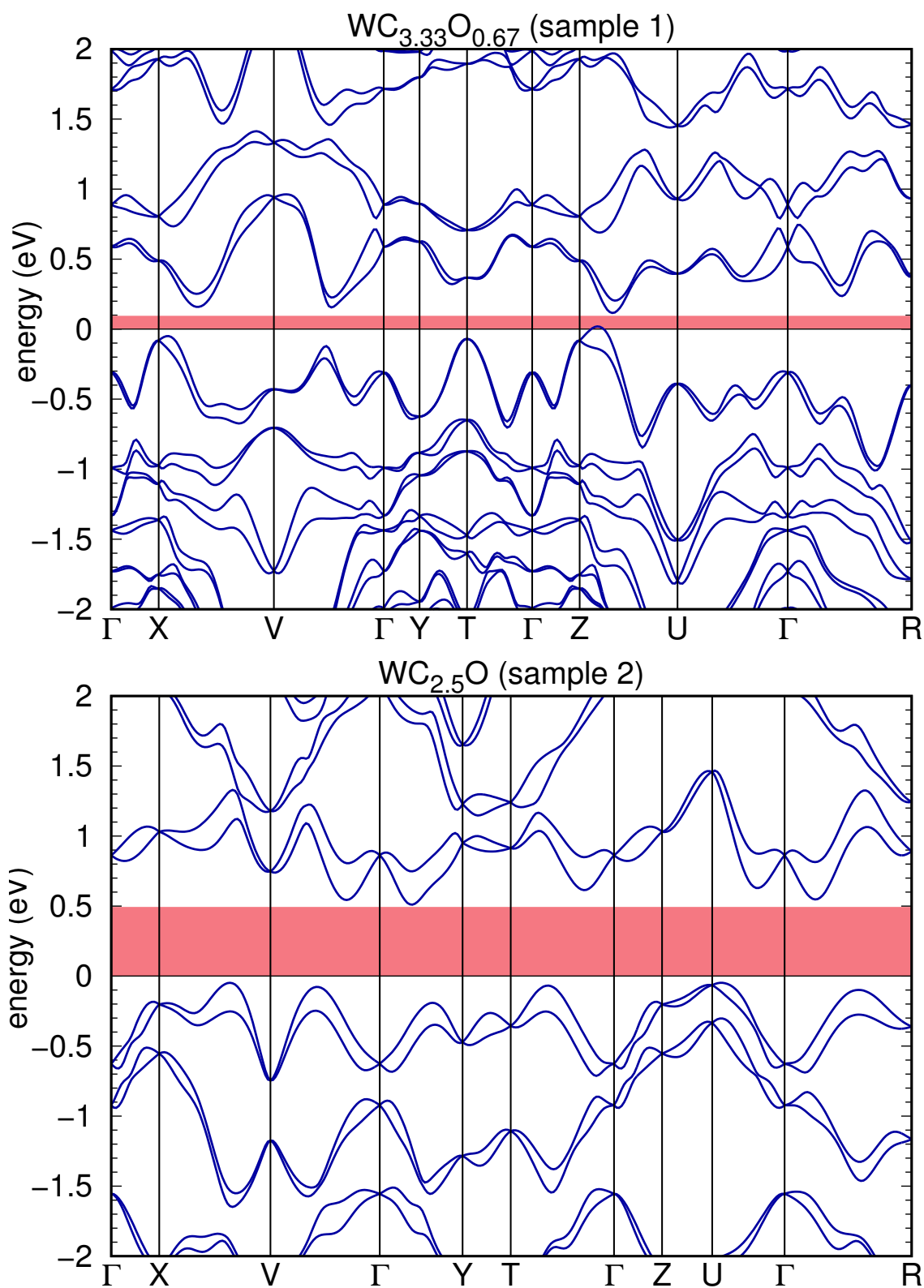


Figure 7. Band structures of the two insulating compounds $WC_{3.33}O_{0.67}$ (top) and $WC_{2.5}O$.

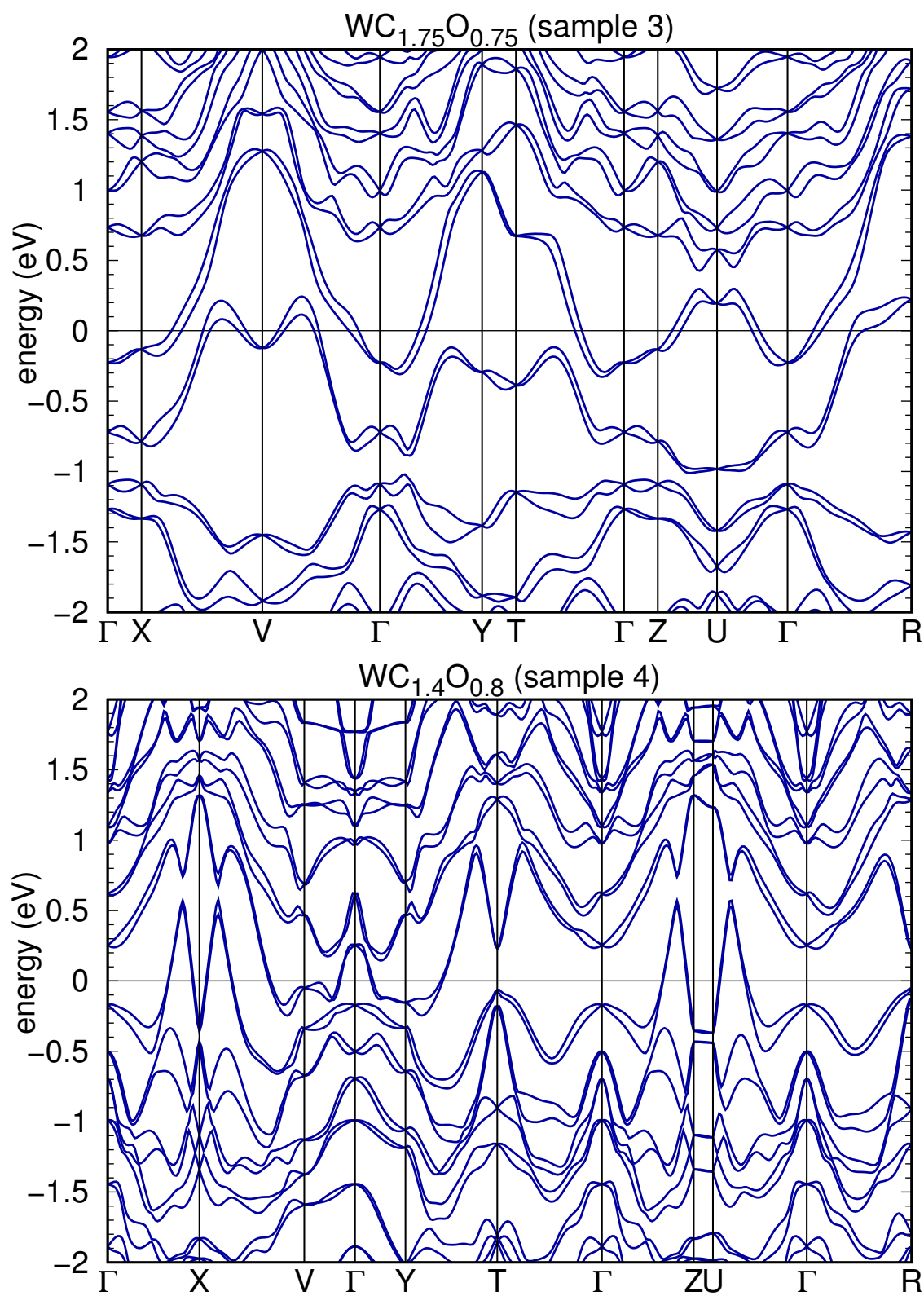


Figure 8. Band structures of two metallic compounds $WC_{1.75}O_{0.75}$ (top) and $WC_{1.4}O_{0.8}$. Compounds with higher relative tungsten content are also metallic.

peak corresponds to bond lengths of 2.5 Å and should be related to tungsten bonds as the light elements contribute only insignificantly to the electron diffraction intensity at 300 keV. Thus, we can relate the electron diffraction pattern to the pair correlation functions of Figs. 9 and 10 and conclude that the W-W bonds most likely cause the electron diffraction peak observed experimentally.

4. Conclusions

By employing evolutionary algorithms we have predicted structures of approximants to EBID-based amorphous tungsten oxycarbides. By analyzing the electronic structure, pair correlation functions and diffraction patterns of our predicted structures for different compositions of W, C and O, we find very good agreement with the experimental observations; an insulator-to-metal transition is observed at a concentration close to the experimental concentration at which this transition is reported and we explain the prominent peak observed in micro-Raman spectroscopy as caused by W-W bonds.

The use of genetic algorithms to predict and simulate amorphous nanodeposits opens the possibility to understand the microscopic origin of the behavior of these systems. This was up to now very limited and mostly restricted to phenomenological models. With this tool at hand, we believe that important progress can be made in this field.

5. Acknowledgments

The authors would like to thank A. Oganov for the generous supply for the code and Q. Zhu for useful discussions and gratefully acknowledge financial support by the Beilstein-Institut, Frankfurt/Main, Germany, within the research collaboration NanoBiC. This work was supported by the Alliance Program of the Helmholtz Association (HA216/EMMI). The generous allotment of computer time by CSC-Frankfurt and LOEWE-CSC is gratefully acknowledged.

References

- [1] Randolph S J, Fowlkes J D and Rack P D 2006 Focused, Nanoscale Electron-Beam-Induced Deposition and Etching *Crit. Rev. Solid State Mater. Sci.* **31** 55
- [2] Cividjian N S-, Hagen C W and Kruit P 2005 Spatial resolution limits in electron-beam-induced deposition *J. Appl. Phys.* **98** 084905
- [3] Porrati F, Sachser R and Huth M 2009 The transient electrical conductivity of W-based electron-beam-induced deposits during growth, irradiation and exposure to air *Nanotechnology* **20** 195301
- [4] Wnuk J D, Rosenberg S G, Gorham J M, van Dorp W F, Hagen C W and Fairbrother D H 2011 Electron beam deposition for nanofabrication: Insights from surface science *Surf. Sci.* **605** 257
- [5] Utke I, Hoffmann P, and Melngailis J 2008 Gas-assisted focused electron beam and ion beam processing and fabrication *J. Vac. Sci. Technol. B.* **26** 1197
- [6] Huth M, Klingenberg D, Grimm C, Porrati F and Sachser R 2009 Conductance regimes of W-based granular metals prepared by electron beam induced deposition *New J. Phys.* **11** 033032

- [7] van Dorp W F, van Someren B, Hagen C W, Kruit P and Crozier A P 2005 Approaching the Resolution Limit of Nanometer-Scale Electron Beam-Induced Deposition *Nano Lett.* **7** 1303
- [8] van Dorp W F and Hagen C W 2008, A critical literature review of focused electron beam induced deposition *J. Appl. Phys.* **104** 081301
- [9] Porrati F, Sachser R, Schwalb C H, Frangakis A S, Huth M 2011, Tuning the electrical conductivity of Pt-containing granular metals by postgrowth electron irradiation *J. Appl. Phys.* **109** 063715
- [10] Donev E U and Hastings J T 2009 Electron-Beam-Induced Deposition of Platinum from a Liquid Precursor *Nano Lett.* **9** 2715
- [11] Shaposhnikov V L, Migas D B, Rodin V N and Borisenko V E 2011 Ab initio investigation of structural and electronic properties of tungsten dioxide *Phys. status solidi (b)* **248** 1471
- [12] Suetin D V, Shein I R, Ivanovskii A L 2010 Tungsten carbides and nitrides and ternary systems based on them: the electronic structure, chemical bonding and properties *Russ. Chem. Rev.* **79** 611
- [13] Tsaur B Y, Mayer J W and Tu K N 1980 Ion-beam induced metastable Pt₂Si₃ phase. I. Formation, structure and properties *J. Appl. Phys.* **51** 5326
- [14] Suetin D V, Shein I R and Ivanovskii A L 2011 Structural, electronic and magnetic properties of tungsten oxycarbides WC_{1-x}O_x and WO_{3-x}C_x from first principles calculations *Phys. Stat. Sol. b* **248** 2884
- [15] Oganov A R, Glass C W 2006 Crystal structure prediction using ab initio evolutionary techniques: Principles and applications *J. Chem. Phys.* **124** 244704
- [16] Glass C W, Oganov A R and Hansen N 2006 USPEX - Evolutionary crystal structure prediction *Comput. Phys. Commun.* **175** 713
- [17] Lyakhov A O, Oganov A R, Valle M 2010 How to predict very large and complex crystal structures *Comput. Phys. Commun.* **181** 1623
- [18] Blöchl P E 1994 Projector augmented-wave method *Phys. Rev. B* **50** 17953
- [19] Kresse G and Joubert D 1999 From ultrasoft pseudopotentials to the projector augmented-wave method *Phys. Rev. B* **59** 1758
- [20] Kresse G and Hafner J 1993 *Ab initio* molecular dynamics for liquid metals *Phys. Rev. B* **47** 558
- [21] Kresse G and Furthmüller J 1996 Efficient iterative schemes for *ab initio* total-energy calculations using a plane-wave basis set *Phys. Rev. B* **54** 11169
- [22] Kresse G and Furthmüller J 1996 Efficiency of ab-initio total energy calculations for metals and semiconductors using a plane-wave basis set *Comput. Mater. Sci.* **6** 15
- [23] Perdew J P, Burke K and Ernzerhof M 1996 Generalized Gradient Approximation Made Simple *Phys. Rev. Lett.* **77** 3865
- [24] Koepernik K and Eschrig H 1999 Full-potential nonorthogonal local-orbital minimum-basis band-structure scheme *Phys. Rev. B* **59** 1743
- [25] Palmer D J and Dickens P G 1979 Tungsten dioxide: structure refinement by powder neutron diffraction *Acta Cryst. B* **35** 2199
- [26] Leciejewicz J 1961 A note on the structure of tungsten carbide *Acta Cryst.* **14** 200
- [27] Porrati F, Sachser R, Strauss M, Andrusenko I, Gorelik T, Kolb U, Bayarjargal L, Winkler B and Huth M 2010 Artificial granularity in two-dimensional arrays of nanodots fabricated by focused-electron-beam-induced deposition *Nanotechnology* **21** 375302

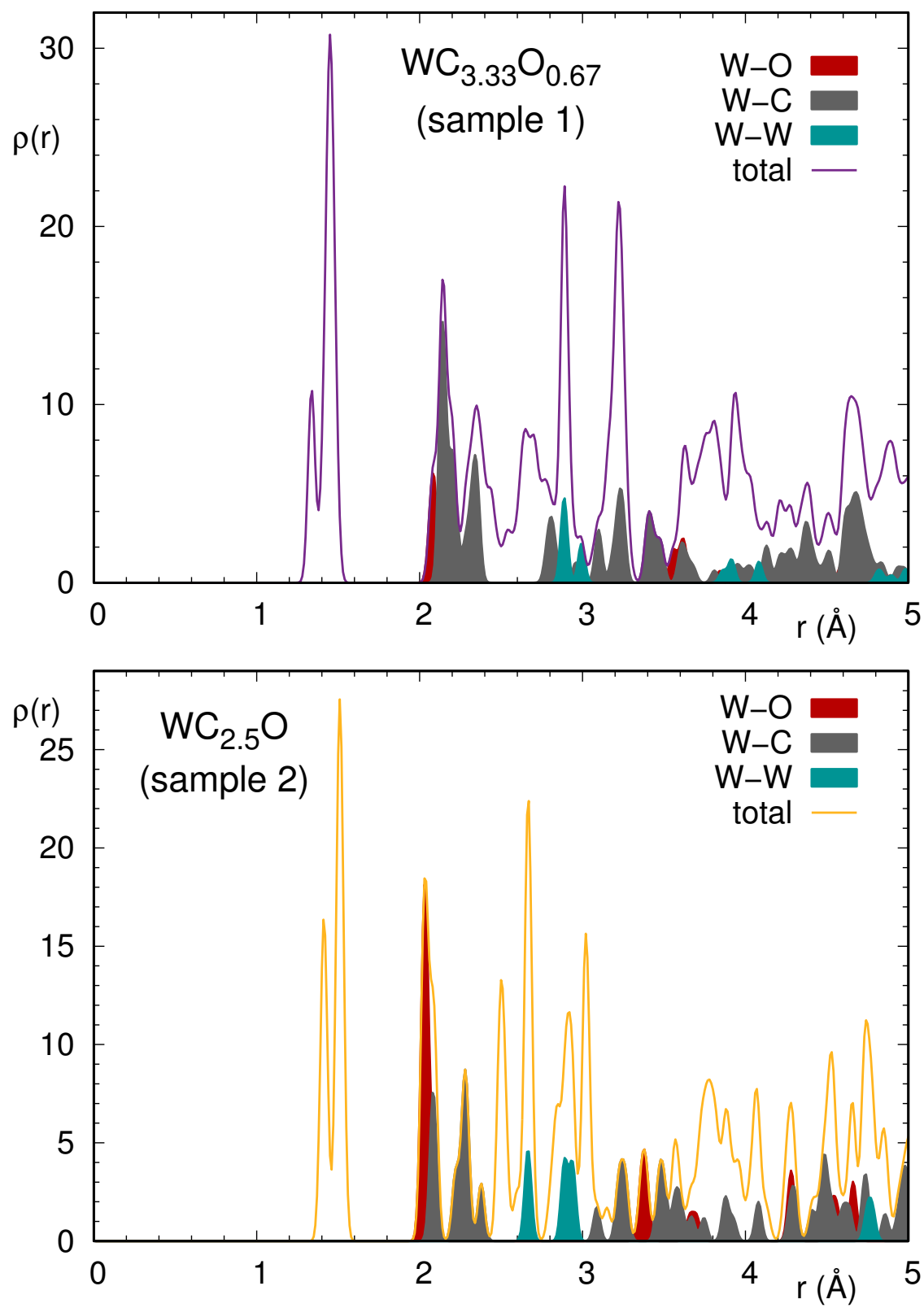


Figure 9. Pair correlation functions of the compounds $WC_{3.33}O_{0.67}$ (top) and $WC_{2.5}O$.

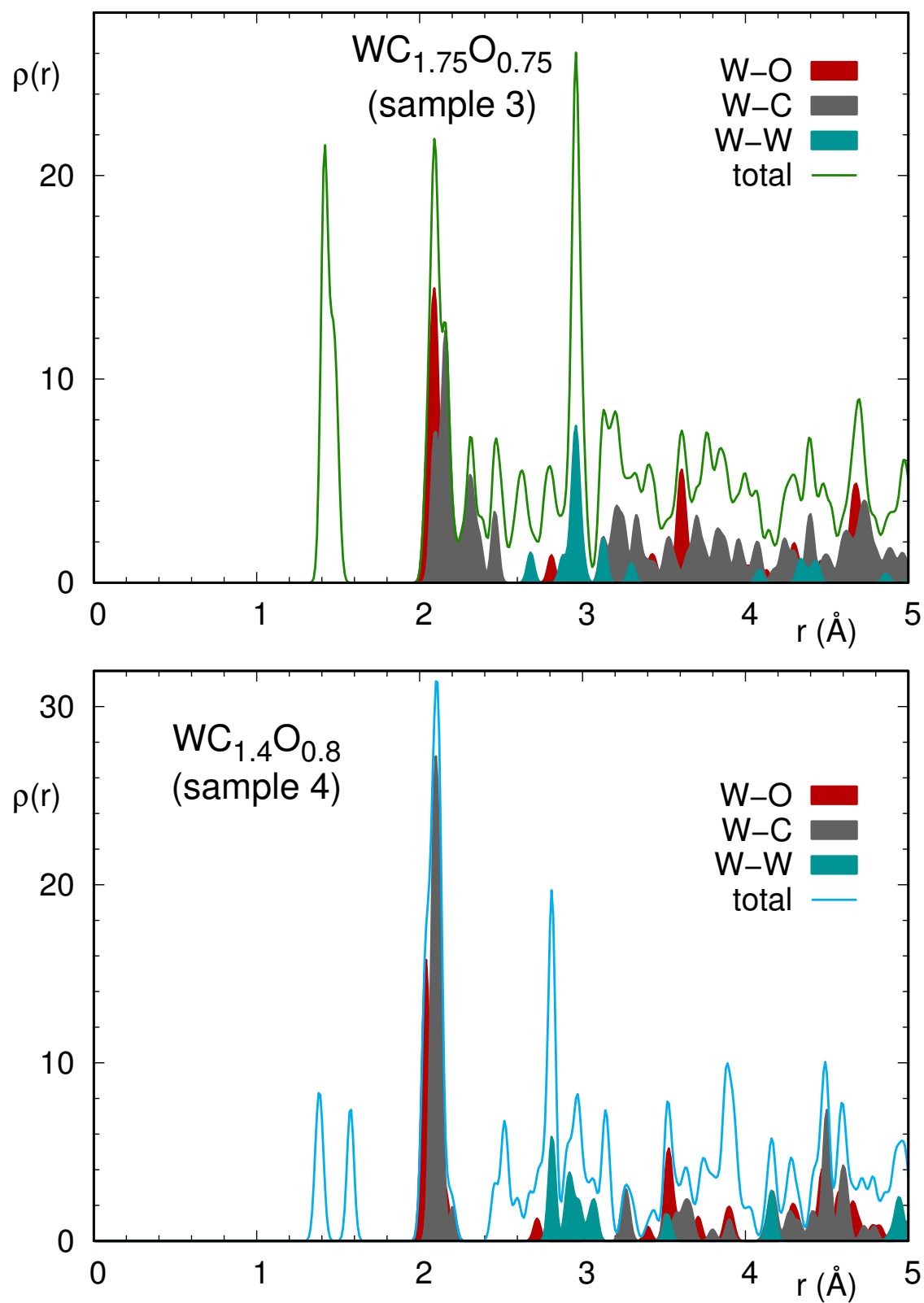


Figure 10. Pair correlation functions of the compounds $\text{WC}_{1.75}\text{O}_{0.75}$ (top) and $\text{WC}_{1.4}\text{O}_{0.8}$.

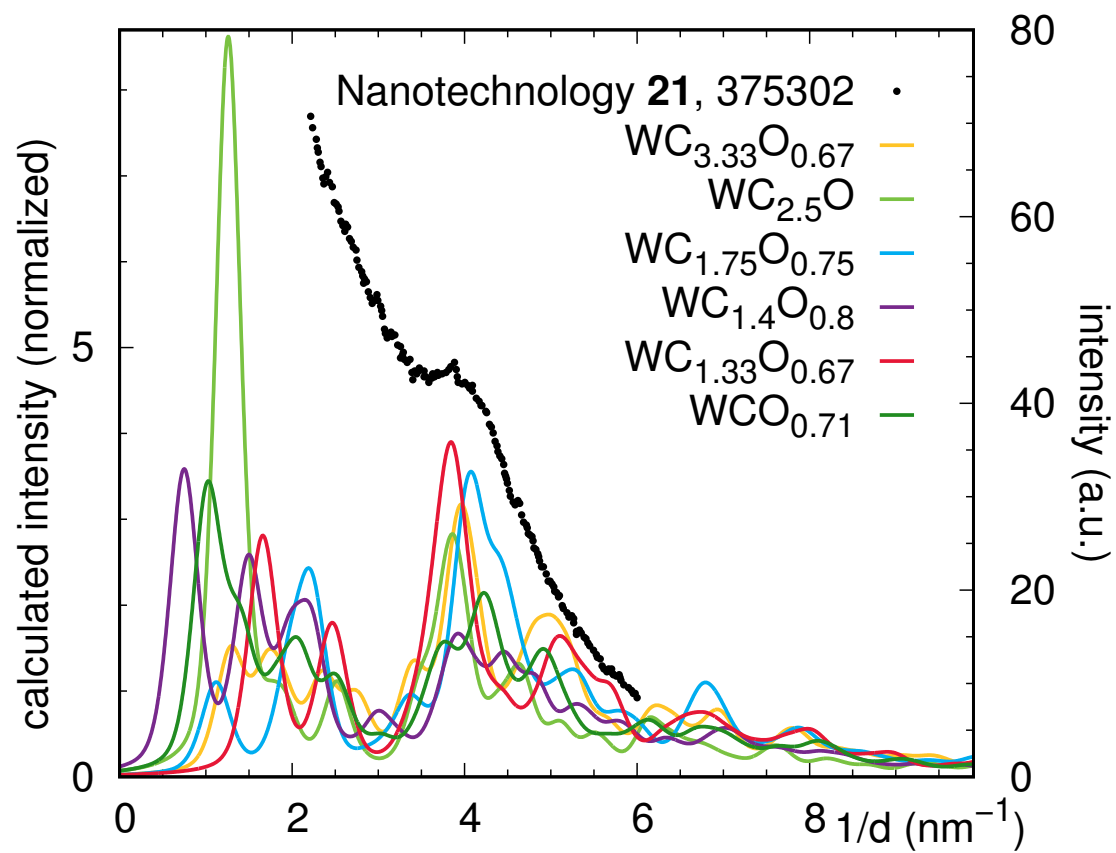


Figure 11. Calculated electron diffraction intensities (lines) for an electron energy of $E = 300$ keV, compared to the measured spectrum of Ref. [27].